Int J Comput Vis
DOI 10.1007/s11263-010-0389-8

Identifying Join Candidates in the Cairo Genizah

Lior Wolf · Rotem Littman · Naama Mayer · Tanya German · Nachum Dershowitz · Roni Shweka · Yaacov Choueka

Received: 25 January 2010 / Accepted: 17 September 2010

Abstract A join is a set of manuscript-fragments that are known to originate from the same original work. The Cairo Genizah is a collection containing approximately 350,000 fragments of mainly Jewish texts discovered in the late 19th century. The fragments are today spread out in libraries and private collections worldwide, and there is an ongoing effort to document and catalogue all extant fragments. The task of finding joins is currently conducted manually by experts, and presumably only a small fraction of the existing joins have been discovered. In this work, we study the problem of automatically finding candidate joins, so as to streamline the task. The proposed method is based on a combination of local descriptors and learning techniques. To evaluate the performance of various join-finding methods, without relying on the availability of human experts, we construct a benchmark dataset that is modeled on the Labeled Faces in the Wild benchmark for face recognition. Using this benchmark, we evaluate several alternative image representations and learning techniques. Finally, a set of newly-discovered join-candidates have been identified using our method and validated by a human expert.

Keywords Cairo Genizah · Document analysis · Similarity learning

L. Wolf (✉) · R. Littman · N. Mayer · T. German · N. Dershowitz
The Blavatnik School of Computer Science, Tel Aviv University, Tel Aviv, Israel
e-mail: wolf@cs.tau.ac.il

R. Shweka · Y. Choueka
The Friedberg Genizah Project, Jerusalem, Israel

1 Introduction

Written text is one of the best sources for understanding historical life. The Cairo Genizah is a unique source of preserved middle-eastern texts, collected between the 11th and the 19th centuries. These texts are a mix of religious Jewish manuscripts with a smaller proportion of secular texts. To make the study of the Genizah more efficient, there is an acute demand to group the fragments and reconstruct the original manuscripts. Throughout the years, scholars have devoted a great deal of time to manually identify such groups, referred to as *joins*, often visiting numerous libraries.

Manual classification is currently the gold-standard for finding joins. However, it is not scalable and cannot be applied to the entire corpus. We suggest automatically identifying candidate joins to be verified by human experts. To this end, we employ modern image-recognition tools such as local descriptors, bag-of-features representations and discriminative metric learning techniques. These techniques are modified for the problem at hand by employing suitable preprocessing and by employing task-specific key-point selection techniques. Where appropriate, we use suitable generic methods.

We validate our methods in two ways. The first is to construct a benchmark for the evaluation of algorithms that are able to compare the images of two leaves. Algorithms are evaluated based on their ability to determine whether two leaves are a join or not. In addition, we create a short list of most likely newly discovered join candidates, according to our algorithm's metric, and send it to a human expert for validation.

The main contributions of this work are as follows:

1. The design of an algorithmic framework for finding join-

Published online: 19 October 2010

candidates. The algorithms are based on the application of local descriptors and machine learning techniques. The framework provides a high-throughput method for join finding in which human expertise is utilized efficiently.

2. The study of suitable algorithmic details for obtaining high levels of performance for finding candidate joins. In particular, by carefully constructing our recognition method, we obtain a considerable increase in recognition rate, at very low false-positive rates.
3. Provide a benchmark for the evaluation of join-finding algorithms. Such a benchmark is important for evaluating such algorithms in the absence of accessible human experts.

Fig. 1 Examples of unknown joins discovered by our system. See text for details

4. The actual identification of new, unknown, joins in the Genizah corpus.

Figure 1 shows a variety of previously-unknown joins discovered by our method. Example (a) consists of two leaves from the same copy of the Mishnah, written on vellum in Hebrew in a square script. The texts are from different tractates of *Order Zeraim*. The left page is from the recently recovered Geneva collection and the right one from the small collection of the Jewish National and University Library. Other leaves from the same manuscript are in Oxford and Cambridge.[1] Example (b) shows fragments from a codex of the Bible, both from the book of Exodus (Hebrew, square script, on vellum), one from Geneva and the other from the Jewish Theological Seminary (JTS) in New York, part of a batch of 69 fragments from various biblical manuscripts (partially vocalized and with cantillation signs). Such codices are written using a very rigid set of typographic rules, and the identification of such joins based on handwriting is considered extremely challenging. Example (c) is in alternating Hebrew and Aramaic (*Targum*, square script), one page from Geneva and the other from the New York JTS collection. Example (d) shows a join of two leaves of Hebrew liturgical supplications from Geneva and from Pennsylvania, in rabbinic script. Example (e) is from a book of precepts of Saadiah ben Joseph al-Fayyūmi, a lost halakhic work by the 10th century gaon. The left page is from the Geneva collection and the right one is from JTS. The language is Judeo-Arabic, and the text is written in a square oriental script on vellum. This join is a good example of how joins can help identify new fragments from lost works. Once one of the pair is identified correctly, the identification of the second one is self-determined. Example (f) is from a responsum in Hebrew (rabbinic script). Both leaves are from the Alliance Israélite Universelle Library in Paris, but they are catalogued under different shelfmarks.

2 Related Work

Genizah Research Discovered in 1896 in the attic of a synagogue in the old quarter of Cairo, the Genizah is a large collection of discarded codices, scrolls, and documents, written mainly in the 10th to 15th centuries. The attic was emptied and its contents have found their way to over fifty libraries and collections around the world. The documents, with few exceptions, are of paper and vellum, and the texts are written mainly in Hebrew, Aramaic, and Judeo-Arabic (in Hebrew characters), but also in many other languages (including Arabic, Judeo-Spanish, Coptic, Ethiopic, and even one in Chinese). The finds included fragments of lost works (such as the Hebrew original of the apocryphal Book of Ecclesiasticus), fragments of hitherto unknown works (such as the Damascas Document, later found among the Qumran scrolls), and autographs by famous personages, including the Andalusians, Yehuda Halevi (1075–1141) and Maimonides (1138–1204).

Genizah documents have had an enormous impact on 20th century scholarship in a multitude of fields, including Bible, rabbinics, liturgy, history, and philology. Genizah research has, for example, transformed our understanding of medieval Mediterranean society and commerce, as evidenced by S.D. Goiten's monumental five-volume work, *A Mediterranean Society*. See Reif (2000) for the history of the Genizah and of Genizah research. Most of the material recovered from the Cairo Genizah has been microfilmed and catalogued in the intervening years, but the photographs are of mediocre quality and the data incomplete (thousands of fragments are still not listed in published catalogues).

The philanthropically-funded Friedberg Genizah Project is in the midst of a multi-year process of digitally photographing (in full color, at 600 dpi) most—if not all—of the extant manuscripts. The entire collections of the Jewish Theological Seminary in New York (ENA), the Alliance Israélite Universelle in Paris (AIU), the Jewish National and University Library (JNUL), the recently rediscovered collection in Geneva, and many smaller collections have already been digitized, and comprise about 90,000 images (recto and verso of each fragment). The digital preservation of another 140,000 fragments at the Taylor-Schechter Genizah Collection at Cambridge is now underway. The images are being made available to researchers online at www.genizah.org.

Unfortunately, most of the leaves that were found were not found bound together. Worse, many are fragmentary, whether torn or otherwise mutilated. Pages and fragments from the same work (book, collection, letter, etc.) may have found their way to disparate collections around the world. Some fragments are very difficult to read, as the ink has faded or the page discolored. Accordingly, scholars have expended a great deal of time and effort on manually rejoining leaves of the same original book or pamphlet, and on piecing together smaller fragments, usually as part of their research in a particular topic or literary work. Despite the several thousands of such joins that have been identified by researchers, very much more remains to be done (Lerner and Jerchower 2006).

Writer Identification A related task to that of join finding is the task of writer identification, in which the goal is to identify the writer by morphological characteristics of a writer's handwriting. Since historical documents are

[1] It turns out that this specific automatically-proposed join has already been discovered and is about to be documented in the Sussmann Catalog and the Geneva catalog, both going into press now.

often incomplete and noisy, preprocessing is often applied to separate the background and to remove noise (see, for instance, Bres et al. 2006; Leedham et al. 2002). Latin letters are typically connected, unlike Hebrew ones which are usually only sporadically connected, and efforts were also expended on designing segmentation algorithms to disconnect letters and facilitate identification. See Casey and Lecolinet (1996) for a survey of the subject. The identification itself is done either by means of local features or by global statistics. Most recent approaches are of the first type and identify the writer using letter- or grapheme-based methods, which use textual feature matching (Panagopoulos et al. 2009; Bensefia et al. 2003). The work of Bres et al. (2006) uses text independent statistical features, and Bulacu and Schomaker (2007), Dinstein and Shapira (1982) combine both local and global statistics.

Interestingly, there is a specialization to individual languages, employing language-specific letter structure and morphological characteristics (Bulacu and Schomaker 2007; Panagopoulos et al. 2009; Dinstein and Shapira 1982). In our work, we rely on the separation of Hebrew characters by employing a keypoint detection method that relies on connected components in the thresholded images.

Most of the abovementioned works identify the writer of the document from a list of known authors. Here, we focus on finding join candidates, and do not assume a labeled training set for each join. Note, however, that the techniques we use are not entirely suitable for distinguishing between different works of the same writer. Still, since writers are usually unknown (in the absence of a colophon or signatures), and since joins are the common way to catalog Genizah documents, we focus on this task. Additional data such as text or topic identification, page size and number of lines can be used to help distinguish different works of the same writer.

The LFW Benchmark To provide a clean computational framework for the identification of joins, we focus in our evaluation on the problem of image pair-matching (same/not-same), and not, for example, on the multiclass classification problem. Specifically, given images of two Genizah leaves, our goal is to answer the following simple question: are these two leaves part of the same original work or not? Previous studies have shown that improvements obtained on the pair-matching problem carry over to other recognition tasks (Wolf et al. 2008).

The benchmark we constructed to evaluate our methods is modeled after the recent Labeled Faces in the Wild (LFW) face image data set (Huang et al. 2007). The LFW benchmark has been successful in attracting researchers to improve face recognition in unconstrained images, and the results show a gradual improvement over time (Huang et al. 2008; Wolf et al. 2008, 2009; Pinto et al. 2009; Taigman et al. 2009; Guillaumin et al. 2009; Kumar et al. 2009), for example; see current results in LFW benchmark results.

3 Overview

The images used in this study along with accompanying catalogical information are provided by the Friedberg Genizah Project. The catalogical information is typically incomplete, and may contain information on the original manuscript, identification of verified joins, page measurements, approximate date, and literature references.

When found in the Genizah, a manuscript leaf might be torn into several fragments and is represented by two or more images depicting the two sides and possibly multiple images of the same side. The images of each leaf fragment are marked recto and verso; however, this marking is generally arbitrary.

The join identification technique follows the following pipeline depicted in Fig. 2. First, the leaf images are preprocessed so that each image is segmented into fragments, and each fragment is binarized and aligned horizontally by rows. In addition, the page is roughly segmented, and various measurements of it are made.

Next, we detect keypoints in the images, and calculate a descriptor for each keypoint. All descriptors from the same leaf are combined, and each leaf is then represented by a single vector. The vectorization is done by employing a "dictionary" which is computed offline beforehand. Finally, every pair of vectors (corresponding to two leaves) are compared by means of a similarity score. We employ both simple and learned similarity scores and, in addition, combine several scores together by employing a technique called stacking.

4 Image Processing and Physical Analysis

The images we obtained from the Friedberg Genizah Project are given as 300–600 dpi JPEGs, of arbitrarily aligned fragments placed on different backgrounds. An example, which is relatively artifact free, is shown in Fig. 3(a). Many of the images, however, contain superfluous parts, such as paper tags, rulers, color tables, etc. (as in Fig. 1). Therefore, a necessary step in our pipeline is preprocessing of the images for separation of fragments from the background and alignment of the fragments by the text rows. Then the physical properties of the fragments and of the text lines are measured.

4.1 Preprocessing

The goal of the preprocessing stage is to eliminate parts of the images that are irrelevant or may bias the join finding process, and to prepare the images for the representation stage.

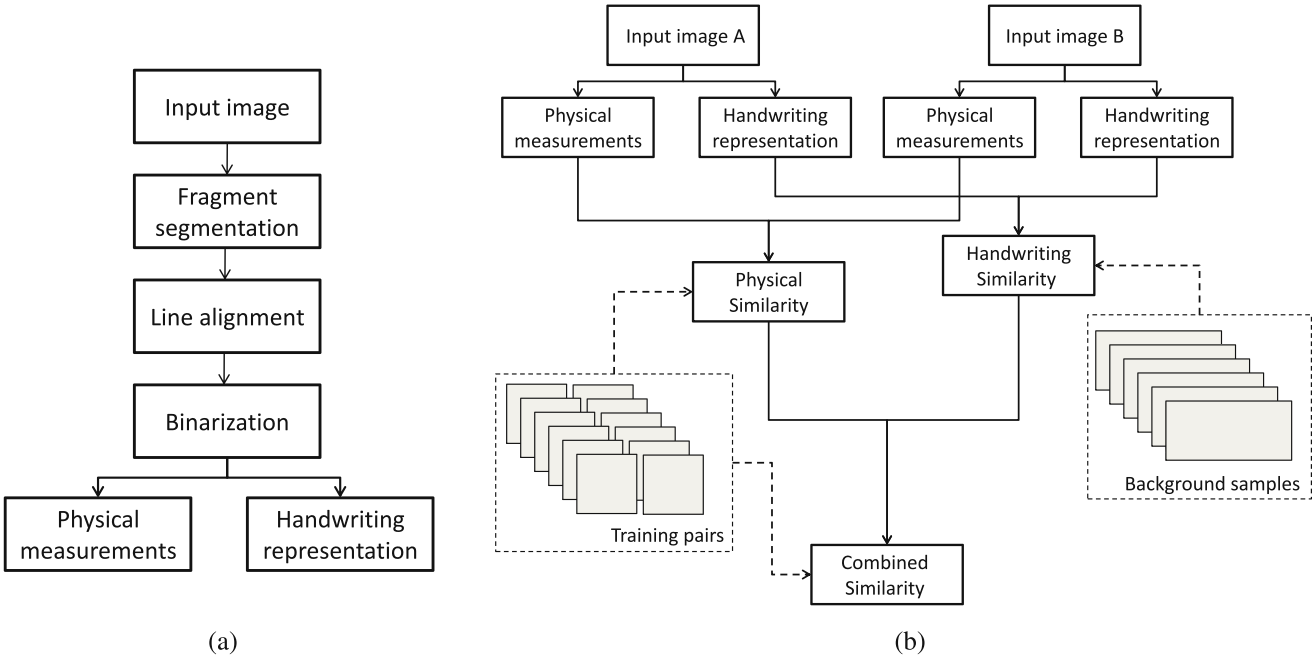

Fig. 2 Overview of the join identification technique. (**a**) The processing of each individual fragment image. The input image is processed to produce a set of physical measurements as well as a bag-of-visual-keywords representation of the handwriting. (**b**) Comparing two images. The background samples are used to compute the One Shot Similarity for the handwriting representations. The combination of the multiple physical measurements and of the multiple similarity scores is done using the stacking techniques that employs positive and negative training pairs

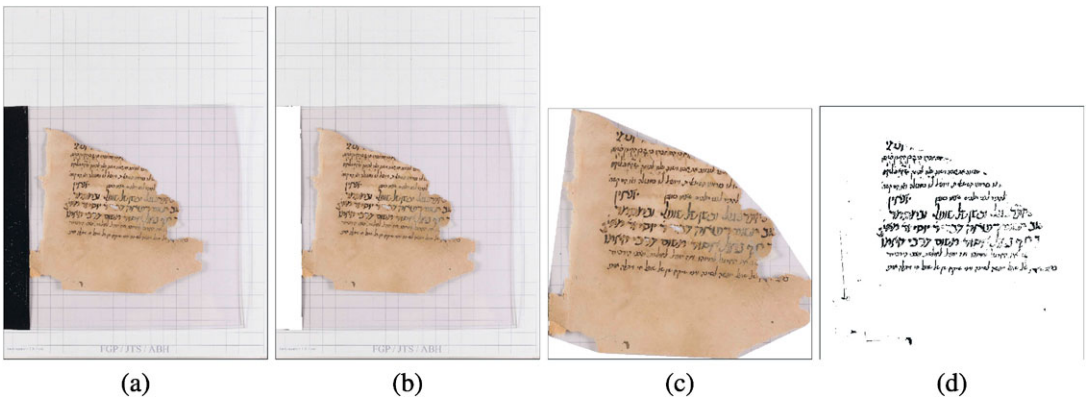

Fig. 3 Example of a document from the Cairo Genizah (ENA collection). (**a**) The original image. (**b**) After removing the black folder binding strip. (**c**) After segmentation (using the convex hull). (**d**) After binarization and alignment

Coarse Manual Alignment In the manual stage, the written sides of each fragment were manually identified. All the images were then manually rotated as necessary in 90° steps, resulting in alignment in the range of $[-45°, 45°]$ from the horizontal direction. This initial rotation prevents the auto-alignment step below from rotating documents upside-down. Note that both the identification of the written side and the coarse alignment stages can be automated; however, the manual effort is not large even for the entire Genizah collection.

Foreground Segmentation The process of separating fragments from their background depends on the way the image was captured. In these experiments we employ images from the AIU, ENA, and JNUL collections. The images of the AIU collection were taken on a distinct cyan graph paper background, and the per-pixel segmentation is performed by a linear SVM classifier that inspects the RGB values of each pixel.

The ENA and JNUL collections are more challenging, since these images vary in backgrounds and are often indis-

tinctive. For example, since the photographs were not taken with automatic analysis in mind, a typical background in those collections may be gray graph paper or blank beige background. Moreover, some of the documents are in plastic sleeves, and some have a black folder stripe on the side. Initial per-pixel segmentation is done by applying three thresholds for each of the three HSV channels. The thresholds are then combined heuristically by a set of rules that focuses mostly on the saturation domain, and then on the value channel.

To create a region-based segmentation of the fragments, we mark the connected components of the detected foreground pixels, and—for ENA and JNUL images—we calculate the convex hull of each component. Those steps retain almost all of the relevant parts of the images, while excluding most of the background.

Detection and Removal of Non-relevant Components Labels, ruler, color swatches, and any other non-relevant components that fall in separated regions are manually removed. In some images, especially large documents, a ruler is adjacent to the actual fragments and is not separated by the region-segmentation process. The ruler used in the images is of a known type, and we locate it by a detector based on correspondence to a reference image of this ruler. The correspondence is done by RANSAC-based (Fischler and Bolles 1981) SIFT (Lowe 2004) keypoint matching. The region of the detected ruler is segmented by color and removed.

In some of the ENA collection images, a black edge of the binder insert sheet holding a fragment (or fragments) is present. In those cases where the binding edge is not separated from the fragment, it is detected in the following manner. The image is binarized using a low threshold over the gray level domain and the edge is recognized for removal as a large rectangular region with very few holes that is adjacent to the image boundary.

Binarization The regions detected in the foreground segmentation process are then binarized using the auto binarization tool of the ImageXpress 9.0 package by Accusoft Pegasus. To cope with failures of the Pegasus binarization, we also binarized the images using the local threshold set at 0.9 of the local average of the 50×50 patch around each pixel. The final binarization is the pixel-wise AND of the two binarization techniques. Pixels near the fragment boundary are set to zero. An example result is shown in Fig. 3(d).

Auto-Alignment Each region is rotated so the rows (lines of text) are in the horizontal direction. This is done using a simple method, which is similar to Baird (1992), Srihari and Govindaraju (1989). We compute the Hough transform of the binary region, as shown in Figs. 4(a) and (b). This gives us the 1D projection profile at each rotation angle, that is equivalent to rotating the image at all angles and summing the pixels along horizontal lines. We then normalize each profile by dividing the Hough transform (point by point) by the Hough transform of the mask of the segmented region that contains the text, to get a normalized Hough transform (Fig. 4(c)–(e)). This normalization is applied since the documents are not guaranteed to be rectangular or to have the same width at each position.

We then calculate the variance of the normalized Hough transform for each angle (Fig. 4(f)), and measure for each angle the local change in this variance. We find the angles of the three points with the highest change, and consider the projection profiles at those three angles. We analyze and score each of the three profiles using the profile score that is described in the physical measurements section (Sect. 4.2). The document is then rotated by the angle that gives the highest profile score.

4.2 Physical Measurements

The measurements that are used in the classification are characteristics of the text rows and dimensions of the text bounding box.

Text Row Measurements The number of text rows, height of the rows, and the spaces between the rows are calculated using the projection profile of the fragment, for each of the three profiles extracted from the normalized Hough transform, as described in the auto-alignment section above. The profile (Fig. 5(b)) is first smoothed using a small (5 pixel) Gaussian filter. Then a moving average is calculated with a window as wide as a quarter of the profile length, that is, a fourth of the height of the aligned fragment. The profile segments that are above the moving average are located, and their mean width is used as a first approximation of the line's height. Then, local projection maxima are located in a neighborhood twice as wide as the approximated text line height (i.e., the segment width). The minimum projection value between every pair of peaks is located, and the profile segment between each pair of neighboring minima is analyzed as a candidate text row. For each such segment i we calculate the following: the value of the peak (Fig. 6(a)); the local height α_i of the peak defined as the difference between the value of the peak and the value of the higher of the two neighboring minima (Fig. 6(b)); the width (W_i) of the stable segment defined as the part of the segment that is over 0.2 its local height (Fig. 6(c)); the number of local peaks in the stable segment (this measurement depends on the writing style and noise); and the number of crossings of the mean of the segment in this stable segment. Segments that do not pass the following criteria are eliminated: the

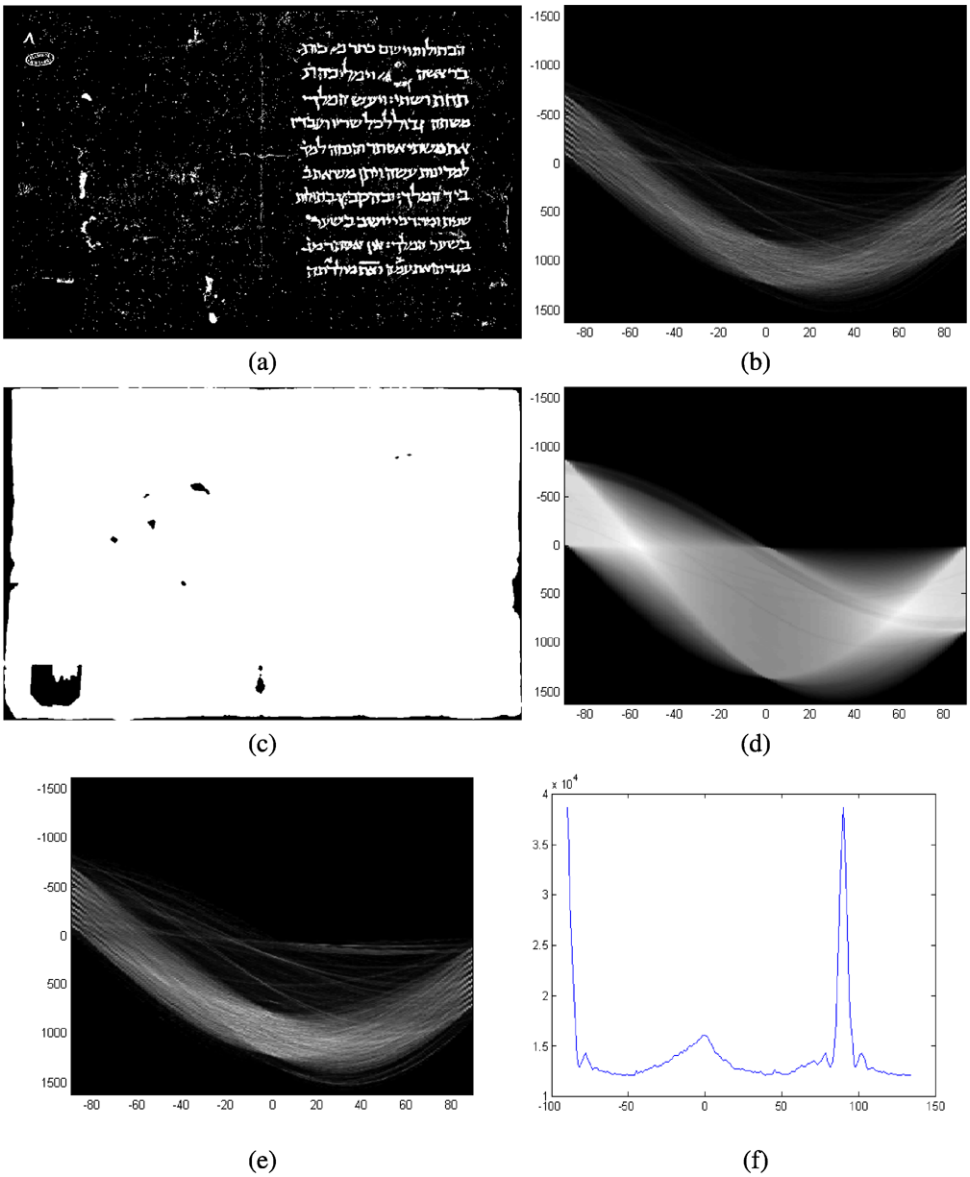

Fig. 4 Hough transform analysis of a fragment. (**a**) Binary image of the fragment. (**b**) Corresponding Hough transform. Note the cyclic pattern around $\pm 90°$ degrees. (**c**) Binary mask of the fragment. (**d**) Corresponding Hough transform. (**e**) Normalized Hough transform. (**f**) The variance of the normalized Hough transform as a function of the angle (the negative part of the angle axis has been duplicated in the positive side for visualization). Note the highest peak around 90°

value and the local height of each peak must be above fixed thresholds, and the number of local peaks and mean crossings for each segment must be below fixed thresholds. Finally, the mean width $\overline{W}$ of the remaining segments is calculated, and only the segments for which $\frac{|\overline{W}-W_i|}{\overline{W}} < 0.75$ (W_i is the width of the ith segment) are considered text rows.

We calculate the average value of the local height measurements α_i for each detected text row. This value is used as the profile score that is used to select the rotation angle out of the three candidates.

The detected text rows, at the selected angle, give rise to several measurements used to identify joins: the number of rows, the mean and standard deviation of the rows' heights (the stable segments' widths), and the mean and standard deviation of the inter-row spaces (the distance between the segments' peaks).

Minimal area Bounding Box The minimal area bounding box is the bounding rectangle of the fragment rotated to the angle where its area is minimal (Fig. 7(a)). It is calculated using the convex hull of the binary mask of the component. For every angle we rotate the points of the convex hull and find their horizontal and vertical span. The angle in which the product of these spans is lowest is selected as the angle of the minimum-area bounding box. In addition, we experimented with computing the dimensions of the axis aligned bounding box, that is, the bounding box of the fragment aligned so that the lines are horizontal (Fig. 7(b)). The dimensions of the minimal area bounding box seem

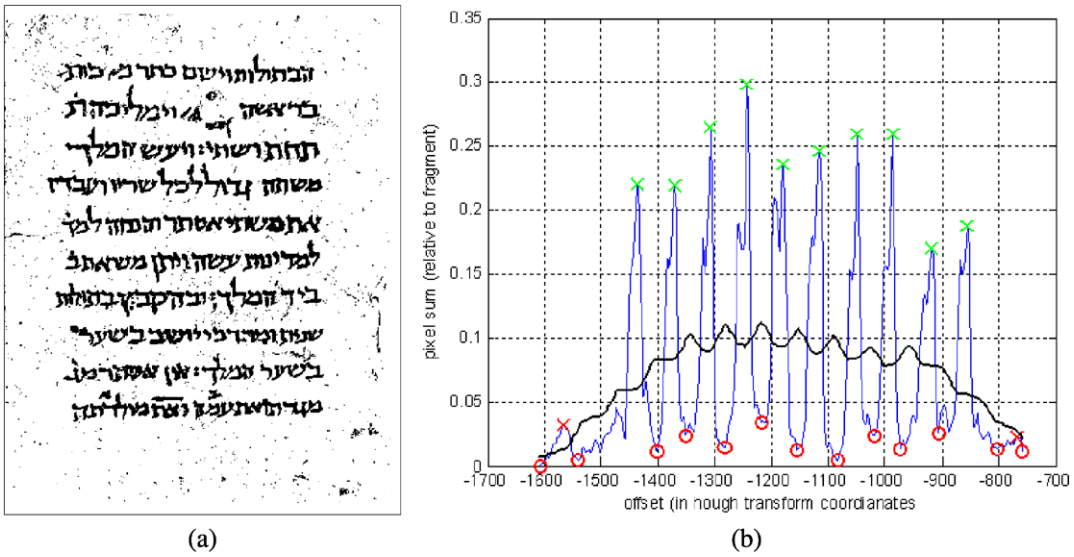

Fig. 5 (Color online) Projection profile. (**a**) Aligned binary fragment. (**b**) Corresponding projection profile. *The dashed black line* is the moving average, *the crosses* are the local maxima, *the green* ones are the final selection and *the red circles* are the minimas between the local maxima

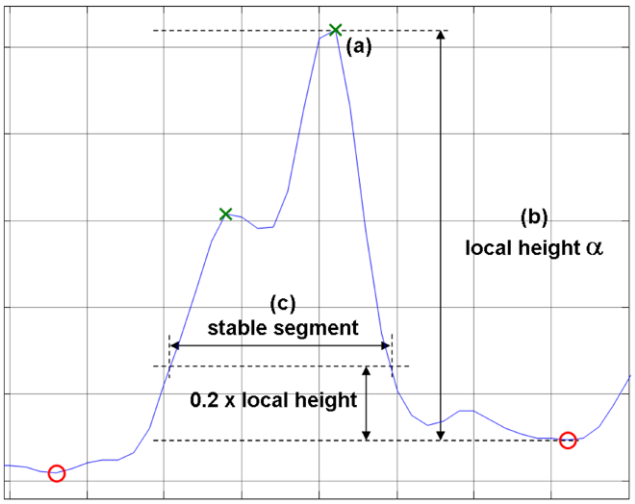

Fig. 6 (Color online) Analysis of a text row segment. (**a**) Segment peak. (**b**) Local height α. (**c**) Stable segment. This segment has two local peaks in its width range (marked by *green crosses*). The surrounding minima are marked by *red circles*

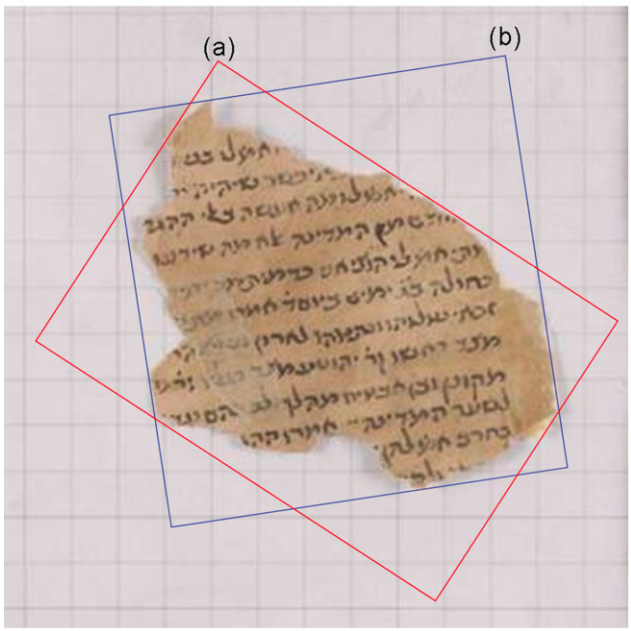

Fig. 7 (**a**) Minimal area bounding box. (**b**) Aligned bounding box

more indicative for join identification than the axis aligned analog.

5 Image Representation

We decided to employ a general framework for image representation that was shown to excel in domains far removed from document processing. Namely, we employ a bag-of-features (Dance et al. 2004; Lazebnik et al. 2006) based method, in which the signature of the leaf is based on descriptors collected from local patches in its fragments, centered around keypoints.

5.1 Keypoint Detection

The simplest method for selecting keypoints, which is often effective in general object recognition tasks (Lazebnik et al. 2006), is to select keypoints on a grid. Grid points are only considered if they belong to the foreground. Another popular method is to employ the Difference of Gaussian (DoG)

(a) (b)

Fig. 8 Keypoint detection methods. (**a**) Using the DoG operator (Lowe 2004). (**b**) Using the proposed CC method

operator used by the SIFT keypoint detector (Lowe 2004). In our experiments with the SIFT detector, we rely on the returned scale of the detector and on the upright direction. We experimented with a few threshold values for the peak threshold parameter, finally selecting 0.005.

A third method for keypoint detection uses the fact that, in Hebrew writing, letters are usually separated. We start by calculating the connected components (CC) of the binarized images. To filter out fragmented letter parts and fragments arising from stains and border artifacts, we compare the size of the CC to the height of the lines which is estimated similarly to the alignment stage above. The scale of each detected keypoint is taken as the maximum dimension of the associated CC.

The CC method has the advantage of using the actual letters of the document; however, the keypoint direction is dependent on correct alignment of fragments (some have multiple line directions), and deals poorly with connected letters. Figure 8 shows the keypoints found using the SIFT and CC detectors.

5.2 Local Descriptors

Each keypoint is described by a descriptor vector. We experimented with the following descriptors: SIFT, PCA-SIFT, binary aligned patch, and binary vertically aligned patch. SIFT (Lowe 2004) and PCA-SIFT (Ke and Sukthankar 2004) are popular descriptors, which encode histograms of gradients in the image. Figure 9 illustrates the application of SIFT to one fragment.

In the binary aligned patch representation, the patch composed of the pixels of the detected keypoint is first stretched to a fixed size of 32×32 pixels, and then the image values are recorded. A somewhat more effective way is to stretch

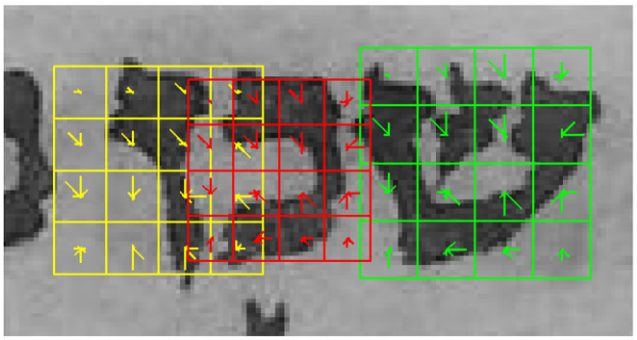

Fig. 9 SIFT descriptors on three neighboring detected keypoints

the patch at the same scale on both axes until the height becomes 32 pixels and then crop or center and zero-pad the resulting patch to a width of 64 pixels.

5.3 Dictionary Creation and Vectorization

Bag-of-feature techniques (Dance et al. 2004) rely on a dictionary that contains a representative selection of descriptors obtained on various interest points. To this end, we set aside a small dataset of 500 documents. We detect keypoints in those documents, by the appropriate method for each experiment, and subsample a large collection of 100,000 descriptors. These are then clustered by the k-means algorithm to obtain dictionaries of varying sizes. Given a dictionary, we employ both histogram-based and distance-based methods to encode each leaf as a vector.

In histogram type vectorization methods (Dance et al. 2004), one counts, for each cluster-center in the dictionary, the number of leaf descriptors (in the encoded image) closest to it. The result is a histogram of the descriptors in the encoded leaf with as many bins as the size of the dictionary. We have experimented with two types of multiplicative normalization. In the first type, we calculate the L2 norm of the resulting vector and divide it by this norm. In the second one, we do the same, by fixing the L1 norm to be 1. While the latter may seem better motivated, in many object recognition systems, it is often the former that performs better.

Distance-based representation techniques (Serre et al. 2005) are based on computing the minimum distance to all descriptors of the given leaf, for each cluster center in the dictionary. We employ two versions. In the first, the distances are used, and in the second we convert distances to similarities by taking the exponential of the distance times -0.001.

6 Similarity Inference

Focusing on just one representation, each leaf is represented by one vector, for example, by the L2 normalized histogram of keypoint types. For every pair of leaves, we need to deter-

mine whether they are from the same join or not. Ideally, we would have a similarity function that would return a high value when two leaves are from the same join, and a low value otherwise. In this ideal case, a threshold over the similarity function provides a decision value.

The basic similarity scores used in this study are based on the L2, L1, and Hellinger norms. The latter is simply the L2 norm applied to the square root of each element in the vector. This norm, similar to the χ^2 norm, is effective for L1 normalized histograms.

We also employ learned similarities. Tailoring similarity measures to available training data by applying learning techniques is gaining popularity; see, for example Bilenko et al. (2004), Cristianini et al. (2002), Hertz et al. (2004), Shental et al. (2006), Weinberger and Saul (2009), Xing et al. (2003). Here, the similarity is to be learned from pairs of samples that are known to belong to the same join or not, and we focus our attention on two types of metric learning methods that have been shown to be successful in the LFW benchmark—one is SVM based, and the other is the LDA-based One Shot Similarity score (OSS).

6.1 SVM of Vector of Absolute Differences

In this technique, which was shown to be effective on the LFW dataset (Pinto et al. 2009), one simply trains an SVM classifier on the vector of absolute differences between the two vectors of every training pair (recall that the training pairs are labeled as positive or negative). Given a new pair, the absolute differences are computed at every coordinate and the trained SVM is applied to the resulting vector. The signed distance from the separating hyperplane is the reported similarity. Higher values indicate better matching leaves.

SVM of Difference and Location The above-mentioned SVM method determines a weighed norm. If a linear SVM is employed, as we do, the method simply produces a weight for each coordinate. The application of the SVM classifier to the vector of absolute differences is equivalent to weighing each coordinate of the two vectors and then computing the L1 norm between the resulting vectors.

The simple form of the learned similarity function has the advantage that it is less prone to overfitting than methods that learn a Mahalanobis metric, such as Bilenko et al. (2004), Cristianini et al. (2002), Weinberger and Saul (2009), Xing et al. (2003); however, it does not take into account the location of the points. The returned similarity score is the same for two vectors $\mathbf{p}$ and $\mathbf{q}$, and for $\mathbf{p}+\mathbf{a}$ and $\mathbf{q}+\mathbf{a}$ for every vector $\mathbf{a}$.

To make the similarity function location-aware, we simply add to the vector representation of each pair the sum of the two vectors. In other words, for a pair of vectors, x and y, the SVM classifier now operates on the vector which is the concatenation of the absolute values of $\mathbf{p}-\mathbf{q}$ and the sum of the two vectors $\mathbf{p}+\mathbf{q}$.

6.2 One Shot Similarity

OSS (Wolf et al. 2008; Wolf et al. 2009) is a similarity learning technique designed for the same/not-same problem. Given two vectors $\mathbf{p}$ and $\mathbf{q}$, their OSS score is computed by considering a training set of background sample vectors $\mathbf{A}$. This set of vectors contains examples of items different from either $\mathbf{p}$ and $\mathbf{q}$ (that is, they do not belong in the same class as either $\mathbf{p}$ nor $\mathbf{q}$). Note, however, that these training samples are otherwise unlabeled. In our experiments, we take the set $\mathbf{A}$ to be one split out of the nine splits used for training at each iteration (see Sect. 7).

A measure of the similarity of $\mathbf{p}$ and $\mathbf{q}$ is then obtained as follows. First, a discriminative model is learned with $\mathbf{p}$ as a single positive example, and $\mathbf{A}$ as a set of negative examples. This model is then used to classify the second vector, $\mathbf{q}$, and obtain a classification score. The nature of this score depends on the particular classifier used. We, following Wolf et al. (2008), employ an LDA classifier, and the score is the signed distance of $\mathbf{q}$ from the decision boundary learned using $\mathbf{p}$ (positive example) and $\mathbf{A}$ (negative examples). A second such score is then obtained by repeating the same process with the roles of $\mathbf{p}$ and $\mathbf{q}$ switched; this time, a model learned with $\mathbf{q}$ as the positive example is used to classify $\mathbf{p}$, thus obtaining a second classification score. The final OSS is the sum of these two scores. It was shown in Wolf et al. (2009) that LDA based OSS can be computed very efficiently. Code for the computation of this similarity is available at http://www.openu.ac.il/home/hassner/projects/Ossk/.

6.3 Classification and Combination of Features

For recognition, we need to convert the similarity values of Sect. 6 to a decision value. Moreover, as in the LFW benchmark, it is beneficial to combine several similarity measures together. For both these tasks we employ linear SVM (fixed parameter value $C=1$), as was done in Wolf et al. (2008, 2006).

In the case of one-similarity, the similarity is fed to the SVM as a 1D vector and training is performed on all training examples. In this case the SVM just scales the similarities and determines a threshold for classification.

To combine several similarities together we use the SVM output (signed distance from hyperplane) obtained from each similarity separately and construct a vector. This vector is then fed to another SVM. The value output by the last classifier is our final classification score. This method of combining classifier output is called stacking (Wolpert 1992). When employing it, care should be taken so that no testing example is used during training. Specifically, the learned

similarities above (SVM-based and OSS) need to be computed multiple times.

7 The Newly Proposed Genizah Benchmark

Our benchmark, which is modeled after the LFW face recognition benchmark (Huang et al. 2007), consists of 31,315 leaves, all from the New York (ENA), Paris (AIU), and Jerusalem (JNUL) collections. There are several differences vis-à-vis the LFW benchmark. First, in the LFW benchmark the number of positive pairs (images of the same person) and the number of negative pairs are equal. In our benchmark, this is not the case, since the number of known joins is rather limited. Second, while in the LFW benchmark, a negative pair is a pair that is known to be negative, in our case a negative pair is a pair that is not known to be positive. This should not pose a major problem, since the expected number of unknown joins is very limited in comparison to the total number of pairs.

There are two views of the dataset: View 1, which is meant for parameter tuning, and View 2, meant for reporting results. View 1 contains three splits, each containing 1000 positive pairs of leaves belonging each to the same join, and 2000 negative pairs of leaves that are not known to belong to the same join. When working on View 1, one trains on two splits and tests on the third.

View 2 of the benchmark consists of ten equally sized sets. Each also contains 1000 positive pairs of images taken from the same joins, and 2000 negative pairs. Care is taken so that no known join appears in more than one set, and that the number of positive pairs taken from one join does not exceed 20.

To report results on View 2, one repeats the classification process 10 times. In each iteration, nine sets are taken as training, and the results are evaluated on the 10th set. Results are reported by constructing an ROC curve for all splits together (the outcome value for each pair is computed when this pair is a testing pair), by computing statistics of the ROC curve (area under curve, equal error rate, and true positive rate at a certain low false positive rate) and by recording average recognition rate for the 10 splits.

7.1 Results Obtained on the New Benchmark

To determine the best methods and settings for join identification, we have experimented with the various aspects of the algorithm. When varying one aspect, we fixed the others to the following default values: the connected component method for keypoint selection algorithm, the SIFT descriptor, a dictionary size of 500, L2 normalized histogram for vectorization, and SVM applied to absolute difference between vectors as the similarity measure.

Results for the parametric methods (keypoint detection method, descriptor type and parameters and dictionary size) were compared on View 1. Results for the various norms and vectorization methods were compared on View 2, since they do not require fitting of parameters.

7.1.1 Parameter Exploration on View 1

Figure 10(a) compares the performance of the various keypoint detectors. For each of the detector types, a new dictionary was created and the entire pipeline was repeated. The

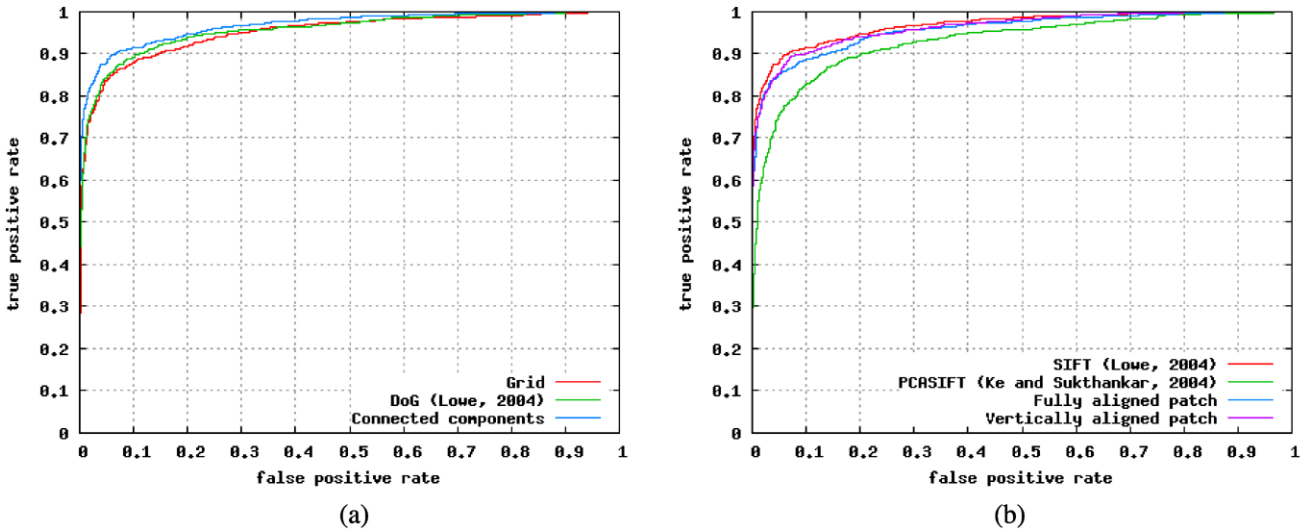

Fig. 10 ROC curves for various keypoint detectors and local descriptors obtained for View 1. (**a**) Results obtained for sampling keypoints on a uniform grid, sampling keypoints according to the DoG method (Lowe 2004), and sampling by the proposed connected components method. (**b**) Results obtained for various local descriptors: SIFT (Lowe 2004), PCA-SIFT (Ke and Sukthankar 2004), and the two proposed patch-based methods

Table 1 Comparison of various vector representations and similarity measures on the View 2 dataset. Four success measures are presented. All scores are averaged over the 10 folds. The standard error (SE) for the mean success rate is omitted for brevity. Typical values for the SE range between 0.005 and 0.01. The four vectorization methods are: bag of keypoint histograms normalized to have a unit L2 norm; similar histogram normalized to have a sum of 1; distance based keypoint representation; and exponential of minus the distance divided by 1000. The norms compared are the L2, L1, and Hellinger norms, as well as SVM scores on the absolute values of the difference between each pair (SVM), a similar SVM method that also takes the location into account (SVM+), and the One Shot Similarity (OSS)

	Area under ROC							Equal error rate					
	L2	L1	Hlngr	SVM	SVM+	OSS		L2	L1	Hlngr	SVM	SVM+	OSS
Hist(L2)	0.9538	0.953	0.9405	0.9600	0.9725	0.9638	Hist(L2)	0.1011	0.1091	0.1275	0.0812	0.0779	0.0808
Hist(L1)	0.9129	0.9413	0.927	0.9527	0.9562	0.9557	Hist(L1)	0.1575	0.1231	0.145	0.1093	0.1048	0.0918
Dist	0.9375	0.9381	0.9405	0.9546	0.9628	0.9731	Dist	0.1243	0.1233	0.1191	0.0994	0.0853	0.0720
Exp(-d)	0.9397	0.9405	0.9387	0.9557	0.9633	0.9733	Exp(-d)	0.1216	0.1199	0.1226	0.0978	0.0834	0.0708
	Mean success (recognition) rate							True positive rate at false positive rate of 0.001					
	L2	L1	Hlngr	SVM	SVM+	OSS		L2	L1	Hlngr	SVM	SVM+	OSS
Hist(L2)	0.9296	0.9199	0.9081	0.9380	0.9409	0.9453	Hist(L2)	0.6772	0.5929	0.5642	0.6387	0.6644	0.7508
Hist(L1)	0.8784	0.9122	0.8915	0.9152	0.9159	0.9374	Hist(L1)	0.3766	0.5869	0.4649	0.5537	0.5283	0.7600
Dist	0.9143	0.9171	0.9191	0.9268	0.9349	0.9501	Dist	0.6074	0.6261	0.6223	0.5814	0.5701	0.7536
Exp(-d)	0.9179	0.9198	0.9164	0.9200	0.9378	0.9503	Exp(-d)	0.6228	0.6351	0.6163	0.6411	0.5840	0.7427

presented results, which are obtained for the best parameters of each of the three methods, demonstrate that the proposed CC based keypoint detector does better than the SIFT DoG keypoint detector. Unlike leading object recognition contributions on datasets such as the Caltech 101 (Lazebnik et al. 2006), placing keypoints on a grid performs worse.

The results of comparing various local descriptors are presented in Fig. 10(b). As can be seen, the SIFT descriptor does better than the patch based descriptors. Given the noisy nature of the underlying images, this is not entirely surprising; however, the PCA-SIFT descriptor did not perform very well. An interesting alternative left for future work, inspired by recent work (Panagopoulos et al. 2009), is to take the outline of the binarized characters in each patch as a descriptor.

The dictionary size seems to have little effect on the results (not shown). For both the histogram based features and the distance based features, performance seemed stable and only slightly increasing when increasing the number of clusters beyond 400. Also omitted is the performance of the exponential of distance based representation for various values of the scale parameter. Performance is pretty stable with regard to this parameter over a large range of values.

7.1.2 View 2 Results

Table 1 depicts the results of the various vectorization methods and similarity measures. It contains one table for each success measure, and within each table one cell for each vectorization/similarity combination. As can be seen, the four vectorization techniques perform mostly similarly. The learned metrics do slightly better than the regular metrics. The location enriched SVM+ learned norm performs very similarly to the SVM norm learned over absolute differences only; however, it does perform better in all measures except for the true positive rate at a very low false positive rate. The One Shot Similarity does better than all other norms in all four measurements. For the most application-crucial measurement of true positive rate at a 0.001 false positive rate, it significantly outperforms (pair t-test $p < 0.05$) all other methods.

The success of the bag-of-feature methods can be compared to the success of the physical measurements approach. We run join identification experiments based on eight physical measurements: number of lines, average line height, standard deviation of line height, average space between lines, standard deviation of interline space, minimal bounding box width, minimal bounding box height, and area of the minimal bounding box. As can be seen in Table 2, these measurements are able to discriminate pretty reliably between joins and random pairs, although not as well as the bag of features approach. We also apply the learned norms to the vectors containing the six measurements, obtaining results that far exceed the results of single measurements. Here, the SVM method is the best performing learned metric.

As can be expected from previous work on the LFW benchmark, combining multiple similarities together improves results. In Table 3 we compare combinations of various groups, all using linear SVM-based stacking (see Sect. 6.3). The combination of the 12 unlearned metrics does

Table 2 Comparison of various physical measurements on the View 2 dataset. The learned metrics SVM, SVM+, and OSS are employed between pairs of 8D vectors containing the physical measurements. Note that since the measurements have outliers, it happens for many of the rows that the SVM classifier used to determine the threshold value sets it such that all examples are predicted as negative. As is clear from the three other scores, using a different threshold, the prediction is not random

Combination	Area under ROC	Equal error rate	Mean success ± standard error	TP rate at FP rate of 0.001
Number of lines	0.6575	0.3803	0.6667 ± 0.0000	0.0000
Average line height	0.8544	0.2062	0.6667 ± 0.0000	0.0076
SD line height	0.7347	0.3152	0.6667 ± 0.0000	0.0023
Average space between lines	0.7278	0.2905	0.6667 ± 0.0000	0.0083
SD space between lines	0.5036	0.5025	0.6667 ± 0.0000	0.0071
Fragment width	0.8442	0.2351	0.6667 ± 0.0000	0.0225
Fragment height	0.8452	0.2350	0.6667 ± 0.0000	0.0257
Fragment area	0.8492	0.2377	0.6667 ± 0.0000	0.0200
SVM	0.9033	0.1843	0.8483 ± 0.0034	0.3596
SVM+	0.9059	0.1779	0.8149 ± 0.0052	0.3171
OSS	0.8662	0.2054	0.8356 ± 0.0052	0.0331

Table 3 Results obtained on View 2 for various combinations of similarity measures. The combinations are (1) L1, L2, or Hellinger norms for histograms normalized by L1 or by L2, distances and the exponential of minus the distances divided by 1000; (2) the four SVM similarities obtained for the two histograms and the two distance based representations; (3) the four One Shot Similarities obtained on the four vector representations; (4) the combination of the best bag-of-features approach with the best physical measurement approach, namely the OSS similarity of L1 normalized distance combined with the SVM based learned metric applied to the eight physical measurements

Combination	Area under ROC	Equal error rate	Mean success ± standard error	TP rate at FP rate of 0.001
All 12 basic norms	0.9661	0.0847	0.9443 ± 0.0032	0.7314
All 4 SVM similarities	0.9715	0.0773	0.9422 ± 0.0035	0.6740
All 4 OSS similarities	0.9754	0.0663	0.9540 ± 0.0028	0.7897
OSS of Hist (L1) + SVM of physicals	0.9785	0.0627	0.9566 ± 0.0028	0.8116

better than any single one. The same is true for the combination of the OSS similarities applied to the four vector representations, and to a lesser extent for the four SVM norms.

Naturally, there is most to be gained by combining metrics that consider separate domains. Indeed, the combination of the best bag-of-features method (OSS of L1 normalized Histogram) and that of the best single physical measurement method (SVM of absolute differences of all six physical measurements) provides the best results. This combination obtains a true positive rate of 81.1% for a false positive rate of 0.1%.

Some of the obtained ROC curves are depicted in Fig. 11(a). While some of the improvements seem incremental, they actually make a significant difference in the low-false positive region (Fig. 11(b)).

8 Newly Found Joins

We have conducted three sets of examinations to evaluate the value of our system in finding joins beyond the settings of the benchmark.

First, we applied the system in order to locate joins in the newly discovered Geneva collection. The search for joins using our tools was pretty efficient, with about 30% of the top 100 matches returned turning out to be actual joins. Examples of our findings for a variety of document categories were given in Fig. 1(a)–(e).

A second set of outside-benchmark experiments was done on an initial benchmark we created for a preliminary version of this work (Wolf et al. 2009). This benchmark was much smaller and contained ten splits each containing 196 positive pairs and 784 negative ones. All images were taken from the ENA and AIU collections. As mentioned above, the negative pairs we work with are not necessarily negative. This does not affect the numerical results much, since the fraction of joins is overall-low; however, it implies that there may exist unknown joins in the set of leaves that are currently available to us.

We applied our classification technique to all possible pairs of leaves and then looked at the 30 leaf pairs that are not known to be joins, but which receive the highest matching scores. The resulting pairs were submitted to a human

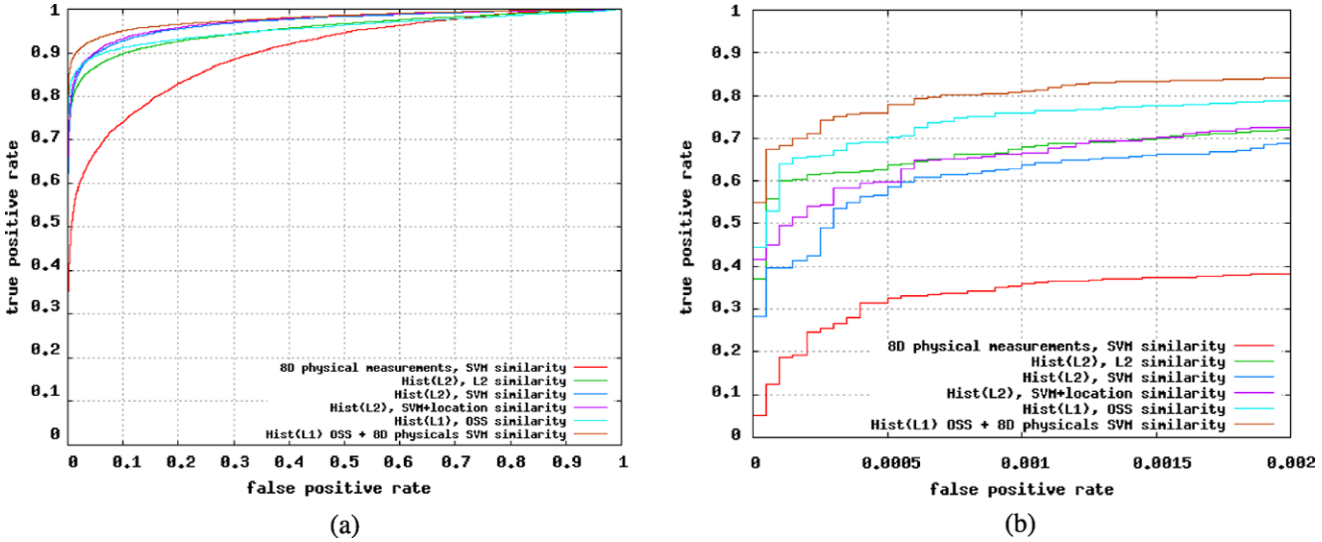

Fig. 11 ROC curves averaged over the 10 folds of View 2. The plots compare the results obtained for the physical measurements (SVM similarity on the 8D vectors); baseline L2 normalized histograms with L2, SVM, and SVM+ similarity; L1 normalized histogram with OSS similarity; and the latter combined with the SVM similarity of the physical measurements. (**a**) Full ROC curvesõ. (**b**) A zoom-in onto the low false positive region

Table 4 Results

Range	Strong join	Weak join	Total join	Excluding empty
1–2000	17.05%	6.95%	24.00%	44.8%
5791–8790	7.16%	6.20%	13.37%	18.0%

expert for validation. The manual labor involved was about 2 and a half hours. The results of this validation are given in the Appendix. Eighty percent of the newly detected join candidates were actual joins. Seventeen percent are not joins, and 1 pair could not be determined.

A third set of join seeking efforts were conducted on all between-collection pairs of fragments unknown to be joins in the ENA, AIU, and JNUL collections, as well as in smaller European collections of mixed quality. Note that inter-collection joins are harder for humans to find, and are more challenging and rare. The top scoring 9,000 pairs were detected. After some further analysis of the catalogical information, some additional known pairs were removed resulting in 8,790 pairs. The first 2,000 pairs and the last 3,000 fragments of this list were studied. The results are given in Table 4. It separates between strong joins, meaning same scribe and same manuscript, and weak joins–same scribe, but believed to originate from different manuscripts. In case of doubt of manuscript identity, though from the same scribe, the pair was marked as a weak join.

As can be seen, 24% of the top discoveries are true joins, mostly strong. More than 13% of the 6th, 7th, and 8th thousands of matches are validated joins. At least half of those are strong joins. Going over the examples it became apparent that many of the found joins are artifacts caused by normalized vectors arising from empty documents. This is to be expected since the benchmark that was used to develop the join discovery tool was not designed to handle blank documents. After the removal of only 49 empty fragments and all their discovered joins, the recognition rates grew considerably.

Overall, through these efforts, approximately one thousand new joins were found. Given that the overall number of joins found in over a century of Genizah research and by hundreds of researchers is only a few thousand, our system has proven its scalability and value. The main limiting factor in finding more joins is the availability of human experts. We hope to alleviate this constraint by making our join candidates available to the Genizah research community.

9 Conclusion and Future Work

We have presented a framework for identifying joins in Genizah fragments, which has already provided value for Genizah researchers by identifying unknown joins. A benchmark has been developed and used for the construction of effective algorithms, borrowing from existing experience in the field of face recognition.

We are making our benchmark, together with the original and processed images and encodings, available for the rest of the community in order to facilitate the effective development of better algorithms in the future.

9.1 Future Work

The high-resolution scanning of the Genizah documents is still taking place, and so far we were able to examine only about 20% of the fragments known to exist, examining less than 4% of the join potential. Note, however, that the methods we employ are efficient and may be employed to the entire corpus in due time.

Our future research plans focus on improving all aspects of the algorithms, as well as including new sources of information such as analysis of the shape of the fragment (fragments of the same join are likely to have the same overall shapes and holes), and the automatic classification of fragment material (paper/vellum).

We are also looking at alternative ways to find similarity between Genizah images. An interesting direction, due to Mica Arie-Nachmison (personal communication), would be to consider patch based composition approaches in comparing two fragments. Two fragment images would be believed to be compatible if one can compose the written area of one image from the written area of another. This is exactly what is being measured by the bidirectional similarity function (Simakov et al. 2008). Initial experiments done with the randomized implementation of Barnes et al. (2009) show that this method might assist in identifying joins; however, the results are still not on a par with the bag-of-features results. The obtained Area Under Curve is 0.63, and the Equal Error Rate is 0.31.

Another avenue of future research is the construction of a paleographic tool that, given a fragment, will provide suitable candidates for matching writing styles and dates. Such a tool will expedite the paleographic classification of the fragments, and will assist the join finding process (the analog in faces would be the recognition of facial traits (Wolf et al. 2009; Kumar et al. 2009) to facilitate better face identification). For the construction of this tool, we plan to use writing samples from various locale and times available in the paleographic literature.

Acknowledgements We would like to thank Dr. Dov Friedberg for a generous grant that enabled us to start this research, and the Friedberg Genizah Project for matching funds that enabled its continuation.

Appendix

The pairs of fragment images below are the top 30 matches of the process described in the paper when applied to all of the pairs that are not known to be joins of the old benchmarks used in Wolf et al. (2009). The last column is the result of the manual classification by a Genizah expert. The results are 24 real joins, 1 not sure and 5 non-joins. We present only one image for each leaf (each leaf may have more than one image: two sides or multiple images of the same side).

Rank	Leaf1	Leaf2	Manual verification	Rank	Leaf1	Leaf2	Manual verification
1			Join	2			Join
3			Join	4			Join
5			Join	6			Join

Rank	Leaf1	Leaf2	Manual verification	Rank	Leaf1	Leaf2	Manual verification
7			Join	8			Join
9			Join	10		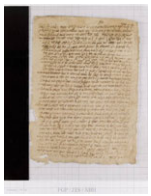	Join
11			Join	12			Join
13			Join	14			Join
15			Join	16			Join
17			Join	18			Join
19			Not join	20			Join
21			Not sure	22			Not join

Rank	Leaf1	Leaf2	Manual verification	Rank	Leaf1	Leaf2	Manual verification
23			Not join	24			Not join
25			Join	26		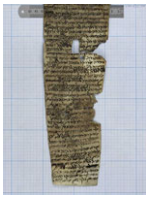	Join
27			Join	28			Join
29			Join	30			Join

References

Baird, K. (1992). Anatomy of a versatile page reader. *Proceedings of the IEEE*, *80*(7), 1059–1065.

Barnes, C., Shechtman, E., Finkelstein, A., & Goldman, D. B. (2009). PatchMatch: a randomized correspondence algorithm for structural image editing. *ACM Transactions on Graphics*, *28*(3) (Proceedings of the SIGGRAPH)

Bensefia, A., Paquet, T., & Heutte, L. (2003). Information retrieval based writer identification. In *Proceedings of the seventh international conference on document analysis and recognition* (pp. 946–950).

Bilenko, M., Basu, S., & Mooney, R. J. (2004). Integrating constraints and metric learning in semi-supervised clustering. In *ICML '04: Proceedings of the twenty-first international conference on machine learning* (p. 11). New York: ACM.

Bres, S., Eglin, V., & VolpilhacAuger, C. (2006). Evaluation of handwriting similarities using hermite transform. In G. Lorette (Ed.), *Tenth international workshop on frontiers in handwriting recognition*. La Baule: Suvisoft.

Bulacu, M., & Schomaker, L. (2007). Automatic handwriting identification on medieval documents. In *Fourteenth international conference on image analysis and processing, ICIAP* (pp. 279–284).

Casey, R., & Lecolinet, E. (1996). A survey of methods and strategies in character segmentation. *IEEE Transactions on Pattern Analysis and Machine Intelligence*, *18*(7), 690–706.

Cristianini, N., Shawe-Taylor, J., Elissee, A., & Kandola, J. (2002). On kernel-target alignment. *Advances in Neural Information Processing Systems*, *14*, 367–373.

Dance, C., Willamowski, J., Fan, L., Bray, C., & Csurka, G. (2004). Visual categorization with bags of keypoints. In *ECCV workshop on statistical learning in computer vision*.

Dinstein, I., & Shapira, Y. (1982). Ancient Hebraic handwriting identification with run-length histograms. *IEEE Transactions on Systerms Man and Cybernetics*, *12*, 405–409.

Fischler, M. A., & Bolles, R. C. (1981). Random sample consensus: a paradigm for model fitting with applications to image analysis and automated cartography. *Communications of the ACM*, *24*(6), 381–395.

Guillaumin, M., Verbeek, J., & Schmid, C. (2009). Is that you? Metric learning approaches for face identification. In *International conference on computer vision*, sep. 2009.

Hertz, T., Bar-Hillel, A., & Weinshall, D. (2004). Boosting margin based distance functions for clustering. In *International conference on machine learning, ICML*, 2004.

Huang, G. B., Ramesh, M., Berg, T., & Learned-Miller, E. (2007). *Labeled faces in the wild: a database for studying face recognition in unconstrained environments*. TR 07-49, UMASS.

Huang, G., Jones, M., & Learned-Miller, E. (2008). LFW results using a combined Nowak plus MERL recognizer. In *ECCV faces in real-life images workshop*.

Ke, Y., & Sukthankar, R. (2004). Pca-sift: a more distinctive representation for local image descriptors. In *Proceedings of the 2004*

IEEE computer society conference on computer vision and pattern recognition, CVPR 2004 (Vol. 2, pp. II–506–II–513)

Kumar, N., Berg, A. C., Belhumeur, P. N., & Nayar, S. K. (2009). Attribute and simile classifiers for face verification. In *IEEE international conference on computer vision, ICCV*, Oct. 2009.

Lazebnik, S., Schmid, C., & Ponce, J. (2006). Beyond bags of features: spatial pyramid matching for recognizing natural scene categories. In *2006 IEEE computer society conference on computer vision and pattern recognition* (Vol. 2, pp. 2169–2178)

Leedham, G., Varma, S., Patankar, A., & Govindarayu, V. (2002). Separating text and background in degraded document images; a comparison of global threshholding techniques for multi-stage threshholding. In *International workshop on frontiers in handwriting recognition* (pp. 244–249).

Lerner, H. G., & Jerchower, S. (2006). The Penn/Cambridge Genizah fragment project: issues in description, access, and reunification. *Cataloging & Classification Quarterly*, *42*(1), 21–39.

LFW benchmark results. http://vis-www.cs.umass.edu/lfw/results.html.

Lowe, D. G. (2004). Distinctive image features from scale-invariant keypoints. *International Journal of Computer Vision*, *60*(2), 91–110.

Panagopoulos, M., Papaodysseus, C., Rousopoulos, P., Dafi, D., & Tracy, S. (2009). Automatic writer identification of ancient Greek inscriptions. *IEEE Transactions on Pattern Analysis and Machine Intelligence*, *31*(8), 1404–1414.

Pinto, N., DiCarlo, J., & Cox, D. (2009). How far can you get with a modern face recognition test set using only simple features? In *IEEE computer society conference on computer vision and pattern recognition*, pp. 2591–2598

Reif, S. C. (2000). *A Jewish archive from Old Cairo: the history of Cambridge University's Genizah collection*. Richmond: Curzon Press.

Serre, T., Wolf, L., & Poggio, T. (2005). Object recognition with features inspired by visual cortex. In *IEEE computer society conference on computer vision and pattern recognition, CVPR* (Vol. 2, pp. 994–1000).

Shental, N., Hertz, T., Weinshall, D., & Pavel, M. (2006). Adjustment learning and relevant component analysis. In *Computer vision, ECCV* (pp. 181–185).

Simakov, D., Caspi, Y., Shechtman, E., & Irani, M. (2008). Summarizing visual data using bidirectional similarity. In *IEEE conference on computer vision and pattern recognition, CVPR 2008* (pp. 1–8).

Srihari, S. N., & Govindaraju, V. (1989). Analysis of textual images using the Hough transform. *Machine Vision and Applications*, *2*(3), 141–153.

Taigman, Y., Wolf, L., & Hassner, T. (2009). Multiple one-shots for utilizing class label information. In *The British machine vision conference, BMVC*, Sept. 2009.

Weinberger, K. Q., & Saul, L. K. (2009). Distance metric learning for large margin nearest neighbor classification. *Journal of Machine Learning Research*, *10*, 207–244.

Wolf, L., Bileschi, S., & Meyers, E. (2006). Perception strategies in hierarchical vision systems. In *2006 IEEE computer society conference on computer vision and pattern recognition* (Vol. 2, pp. 2153–2160).

Wolf, L., Hassner, T., & Taigman, Y. (2008). Descriptor based methods in the wild. In *Faces in real-life images workshop in ECCV*.

Wolf, L., Hassner, T., & Taigman, Y. (2009). The one-shot similarity kernel. In *IEEE international conference on computer vision, ICCV*, Sept. 2009.

Wolf, L., Littman, R., Mayer, N., Dershowitz, N., Shweka, R., & Choueka, Y. (2009). Automatically identifying join candidates in the Cairo Genizah. In *Post ICCV workshop on eHeritage and digital art preservation*, Sept. 2009.

Wolf, L., Taigman, Y., & Hassner, T. (2009). Similarity scores based on background samples. In *Asian computer vision conference, ACCV*, Sept. 2009.

Wolpert, D. H. (1992). Stacked generalization. *Neural Networks*, *5*(2), 241–259.

Xing, E., Ng, A. Y., Jordan, M., & Russell, S. (2003). Distance metric learning, with application to clustering with side-information. In *NIPS*.